doi:10.2533/chimia.2024.762 Chimia 78 (2024) 762–770

Fine Particle pH and Sensitivity to NH_3 and HNO_3 over South Korea During KORUS-AQ

Ifayoyinsola Ibikunle[a], Andreas Beyersdorf[b], Pedro Campuzano-Jost[c,d], Chelsea Corr[b+], John D. Crounse[e], Jack Dibb[f], Glenn Diskin[g], Greg Huey[h], Jose-Luis Jimenez[c,d], Michelle J. Kim[e], Benjamin A. Nault[c,d,$], Eric Scheuer[f], Alex Teng[e], Paul O. Wennberg[e], Bruce Anderson[b], James Crawford[b], Rodney Weber,[h*] and Athanasios Nenes[h,i,j*]

Abstract: Using a new approach that constrains thermodynamic modeling of aerosol composition with measured gas-to-particle partitioning of inorganic nitrate, we estimate the acidity levels for aerosol sampled in the South Korean planetary boundary layer during the NASA/NIER KORUS-AQ field campaign. The pH (mean ± 1σ = 2.43±0.68) and aerosol liquid water content determined were then used to determine the 'chemical regime' of the inorganic fraction of particulate matter (PM) sensitivity to ammonia and nitrate availability. We found that the aerosol formation is always sensitive to HNO_3 levels, especially in highly polluted regions, while it is only exclusively sensitive to NH_3 in some rural/remote regions. Nitrate levels are further promoted because dry deposition velocity is low and allows its accumulation in the boundary layer. Because of this, HNO_3 reductions achieved by NO_X controls prove to be the most effective approach for all conditions examined, and that NH_3 emissions can only partially affect PM reduction for the specific season and region. Despite the benefits of controlling PM formation to reduce ammonium-nitrate aerosol and PM mass, changes in the acidity domain can significantly affect other processes and sources of aerosol toxicity (*e.g.* solubilization of Fe, Cu and other metals) as well as the deposition patterns of these trace species and reactive nitrogen.

Keywords: Aerosol acidity · Ambient measurements · Nitrate · Thermodynamics

Ifayoyinsola ("Yoyin") Ibikunle, graduate student at the School of Earth and Atmospheric Sciences, Georgia Institute of Technology, Atlanta Georgia. Her research focuses on atmospheric acidity and its impacts on aerosol formation.

Prof. Athanasios Nenes, Ecole Polytechnique Fédérale de Lausanne, Switzerland. Director of the Laboratory of Atmospheric Processes and their impacts, affiliated Scientist and co-director of the Center for the Study of Air Quality and Climate Change at the Foundation for Research and Technology Hellas (Patras, Greece). Research focuses on the impact of atmospheric processes on clouds, climate, air quality and ecosystems. He is the prime author of the ISORROPIA aerosol thermodynamics models, aerosol-cloud interaction parameterizations, and developer of instrumentation to measure cloud condensation nuclei. Highly cited researcher in geosciences, he served as president of Atmospheric Sciences of the European Geophysical Union, is an expert of the IPCC AR7 WG1, served on of the UN Joint Group of Experts on the *Scientific Aspects of Marine Environmental Protection*, and the US National Academies Committee on the *Future of Atmospheric Chemistry Research*. American Geophysical Union (AGU) Fellow, American Association for Aerosol Research (AAAR) Fellow. Recipient of the Copernicus Medal, Ascent Award from the Atmospheric Sciences Section of the AGU, AAAR Sinclair, Whitby and Friedlander Awards, American Meteorological Society Houghton Award.

Prof. Rodney Weber is a professor of Atmospheric Chemistry at School of Earth & Atmospheric Sciences at the Georgia Institute of Technology in Atlanta, GA, USA. He has made seminal contributions on the topics of New Particle Formation, Secondary Organic Aerosol Formation, Aerosol and Human Health Effects, Fine Particle Acidity and Aerosol Brown Carbon. He is the inventor of the Particle-Into-Liquid Sampler (PILS) and is a highly cited researcher in the field of Geosciences, and distinctions include the Kenneth T. Whitby Award from the American Association for Aerosol Research, and the Ascent Award from the Atmospheric Sciences Section of the American Geophysical Union.

*Correspondence: Prof. A. Nenes, E-mail: athanasios.nenes@epfl.ch; Prof. R. Weber, E-mail: rweber@eas.gatech.edu
[a] School of Chemical and Biomolecular Engineering, Georgia Institute of Technology, Atlanta, GA 30332, USA;[b]NASA Langley Research Center, Hampton, VA 23681, USA; [c]Department of Chemistry, University of Colorado, Boulder, CO 80309, USA; [d]Cooperative Institute for Research in Environmental Sciences, University of Colorado, Boulder, CO 80309, USA; [e]California Institute of Technology, Pasadena, CA 91125; [f]Institute for the Study of Earth, Oceans, and Space, University of New Hampshire, Durham, NH 03824, USA; [g]NASA Ames Research Center, Moffett Field, CA 94035, USA; [h]School of Earth and Atmospheric Sciences, Georgia Institute of Technology, Atlanta, GA 30332, USA; [i]School of Architecture, Civil & Environmental Engineering, Ecole Polytechnique Fédérale de Lausanne, CH-1015, Lausanne, Switzerland; [j]Center for the Study of Air Quality and Climate Change, Institute for Chemical Engineering Sciences, Foundation for Research and Technology Hellas, Patras, GR-26504, Greece; [+]Currently at Colorado State University; [$]Currently at Center for Aerosol and Cloud Chemistry, Aerodyne Research Inc., Billerica, MA, USA

1. Introduction

Poor air quality from high concentrations of fine particulate matter over South Korea has its origin in domestic emissions from vehicles, industry, and biomass burning, combined with long-range transport of pollutants from mainland China.[1,2] Because air quality in South Korea is a mixture of factors such as regional and local emissions from both anthropogenic and natural (*e.g.* dust) sources, as well as meteorological (*e.g.* wind, relative humidity) and chemical interactions (*e.g.* photochemistry), assessing possible air pollution control strategies in this region is challenging.[3]

To improve our understanding of poor air quality in South Korea, the Korean National Institute of Environmental Research (NIER) and the United States National Aeronautics and Space Administration (NASA), conducted a field study in South Korea from 26th April to 18th June 2016.[3] The aim of the Korea-United States Air Quality Study (KORUS-AQ), was to determine the factors that contribute to the poor regional air quality to aid the development of effective air quality mitigation strategies.

During the KORUS-AQ campaign, secondary production of particulate matter (PM) – organic and inorganic – constitute a significant fraction of PM pollution, with significant contribution from local sources. Since sulfate and nitrate comprised nearly half of the mass of PM at sizes smaller than 1 μm (PM_1),[2,4] aerosol acidity, liquid water content and temperature will significantly affect aerosol properties including its mass through the gas-particle partitioning of semi-volatile species.[5] More broadly, fine aerosol particle acidity in South Korea affects air quality and human health and therefore requires knowledge of aerosol pH levels (*e.g.* refs. [5,6]).

Given that direct measurement of atmospheric aerosol pH remains a challenge, there is large uncertainty in this important parameter.[6] Of all approaches used to date for constraining aerosol pH, use of thermodynamic analysis of gas-aerosol observations together with a model provides the most robust estimates of aerosol acidity.[6-8] To achieve the most robust pH predictions, thermodynamic analysis requires observations of all species, both gas and particle phase, that affect pH. Knowledge of gas-phase ammonia and particulate ammonium is especially important, owing to its role as the dominant cation in fine-mode aerosol and pH-sensitive partitioning. Accurate measurement of ammonia, especially at low concentrations, is far from trivial[9,10] and subject to biases from adsorption of NH_3 in instrument inlets and NH_4^+ volatilization.[11-14] Although aerosol NH_4^+ measurements are common, measurements of gas-phase NH_3 are often missing in field studies – including for KORUS-AQ. There is a need to accurately infer aerosol pH in the absence of gas-phase NH_3 data.

This study aims to accurately determine fine particle pH for aerosol in South Korea and use this inferred pH to understand the sensitivity of PM mass to the availability of ammonia and nitric acid (which are two major aerosol precursors). Focusing only on the inorganic fraction of the aerosol, we develop a computationally rigorous approach to estimate aerosol pH and particle liquid water despite missing gas-phase ammonia data and apply it to the KORUS-AQ dataset. We then utilize these data to assess optimal strategies to control inorganic aerosol mass through reduction of either available nitric acid or ammonia, based on the new approach from ref. [5]

2. Analysis

Observations were obtained from instruments operated on an airborne platform, described below. Flight details are given in Section 3 along with data and their interpretation.

2.1 *Instrumentation*

Non-refractory PM_1 Composition

The CU-Boulder highly customized Aerodyne high-resolution time-of-flight aerosol mass spectrometer (HR-ToF-AMS) measured non-refractory (NR) PM_1 composition, including ammonium, nitrate, sulfate, chloride, and organic aerosol. The basic concept, operation, and aircraft deployment of the AMS has been described elsewhere[15-17] and the deployment for KORUS-AQ is discussed in detail in ref. [2]. Observations are reported in units of μg sm^{-3} (under standard conditions of T=273.15 K, p=1013 hPa). For the following analysis, the data were converted to concentrations at ambient conditions for the thermodynamic calculations.

The AMS also separately measures the contribution of amines, organonitrates and organosulfates.[18-20] During the campaign, organic nitrates comprised roughly 8% of the AMS particulate NO_3 signal and were only an important contribution to the signal when NO_3 was below 0.50 μg sm^{-3} (0.45 μg m^{-3}).[2] Average concentration of nitrate during the campaign was 8.09 ± 6.16 μg m^{-3}, so we consider AMS nitrate to be approximately equal to inorganic aerosol NO_3^-. Accuracy (2σ) for AMS detection of inorganic species is estimated to be 35%.[21]

Gas-phase HCl and HNO_3

HCl and HNO_3 measurements were made using the Georgia Institute of Technology Chemical Ionization Mass Spectrometer (GT CIMS) and the California Institute of Technology CIMS (CIT CIMS), respectively. The GT CIMS technique utilizes a low-pressure ion source/reactor and SF_6^- reagent ion chemistry to detect HCl.[22,23] The CIT CIMS utilizes CF_3O^- chemistry to detect HNO_3 by way of fluoride transfer.[24-26] Both methods are configured to allow for ion chemistry in a heated Teflon-coated flow tube at low pressure to selectively cluster the reagent ions with HNO_3 (HCl) in ambient air.[22] The ions from the flow tube enter a mass spectrometer, where they are mass-analyzed and quantified. Gas-phase concentrations were reported in ppbv (parts-per-billion, by volume), and were subsequently converted to μg m^{-3} at ambient conditions prior to thermodynamic analysis. The estimated CIMS measurement uncertainty is 40%.

Non-volatile Aerosol Cations and Meteorological Variables

Non-volatile cations (NVCs), such as Na^+, K^+, Ca^{2+}, and Mg^{2+}, were measured using the soluble acidic gases and aerosols (SAGA) instrumentation. Bulk aerosol (nominally < 4.1 μm aerodynamic diameter) are collected onto filters to quantify soluble ions.[27] Detection limits are 5 pptv for Mg^{2+} and better than 20 pptv for Na^+, K^+, and Ca^{2+} (https://cloud1.arc.nasa.gov/docs/intex-b/SAGA_Dibb.pdf). Filter sampling times were approximately 5 min or less. Units of NVCs were reported in μg m^{-3} under ambient conditions when used for thermodynamic calculations. Water vapor content was measured using a diode laser hygrometer[28] and then converted to relative humidity based on the measurement of temperature measured onboard.

2.2 *Thermodynamic Analysis of Observations and PM Sensitivity to Aerosol Precursors*

ISORROPIA-II[29] (http://isorropia.epfl.ch), was used to calculate the equilibrium phase state and composition of inorganic aerosol systems containing NH_4^+, SO_4^{2-}, NO_3^-, Cl^-, Na^+, Ca^{2+}, K^+, Mg^{2+}, aerosol liquid water content, and partitioning of semi-volatile species (*e.g.* particle nitrate, NO_3^-, and gas phase nitric acid, HNO_3). ISORROPIA-II was run in forward mode, which results in more robust and accurate predictions of pH owing to the sensitivity of reverse mode calculations to measurement uncertainty.[7,8] The model assumes that fine particles and their corresponding volatile counterparts are in thermodynamic equilibrium, which is a good assumption for submicron particles that are not kinetically limited by size (*i.e.* in the fine mode)[30,31] and slow diffusivity in the particle phase. For the selected KORUS-AQ dataset (<1 km ASL, 45% < relative humidity (RH) < 95%, average RH: 62±12%; average temperature: 20.2±2.5 °C) the aerosol tends to be in a liquid metastable state (*i.e.* no precipitation of salts

under supersaturated conditions.[29,32,33] Efflorescence typically occurs for RH between 10-30%, however, such humidity points were not considered in our analysis.

While ISORROPIA II can handle systems containing non-volatile cations (NVCs), such as Na^+, K^+, Mg^{2+}, and Ca^{2+}, they were not considered in the analysis owing to their very low concentration (Fig. 1) and minor impact on aerosol pH;[14] as well as the fact that much of the NVCs were in the super-micron mode.[34,35] A sensitivity calculation, using SAGA measurements (as it includes aerosol with size less than 4.1 μm) as an upper limit of submicron NVCs pH confirms this (Table S1).

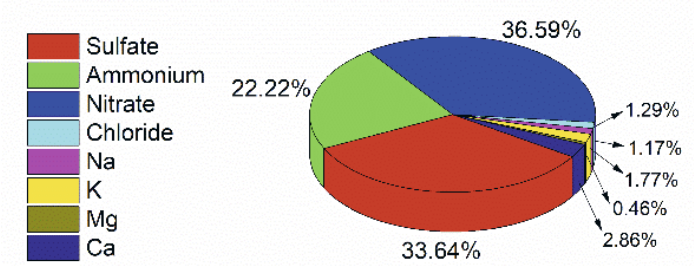

Fig. 1. Average inorganic PM_1 mass composition throughout the entire study and for altitudes below 1km. Average total mass is 22 μg m^{-3}.

ISORROPIA II is used to calculate the pH of aerosols. pH is defined as:

$$pH = -log_{10}(\gamma_{H^+} H^+_{aq}) = -log_{10}(\frac{1000\,\gamma_{H^+}\,H^+_{air}}{W_i+W_o}) \approx -log_{10}(\frac{1000\,\gamma_{H^+}\,H^+_{air}}{W_i}) \quad (1)$$

where γ_{H^+} is the hydronium ion activity coefficient – here assumed to be unity, H^+_{aq} (mol L^{-1}) hydronium ion concentration in aerosol liquid water, H^+_{air} (μg m^{-3}) hydronium ion concentration per volume of air, and W_i (μg m^{-3}) and W_o (μg m^{-3}) are the particle liquid water concentrations associated with inorganic and organic species, respectively. Although W_o can be estimated, *e.g.* through the hygroscopicity parameter,[36] its effect on pH, together with organic effects on the activity coefficient, are secondary - introducing somewhere between a 0.15 and 0.30 pH units change.[8,36,37] Note Equation 1 is consistent with the 'pH_F' definition of ref. [6].

As applied here, the thermodynamic analysis provides pH consistent with 'bulk' pH, which assumes that particles are internally mixed. This assumption tends to provide good estimates of pH for submicron particles, given that the equilibrium assumption is largely satisfied and semi-volatile partitioning of gases such as NH_3 and HNO_3 is well captured.[6,38] Internal mixing is achieved in a few hours in polluted areas due to rapid secondary aerosol production.[39,40] Both the ground AMS[1] and the aircraft AMS[2] saw no evidence of external mixing based on the mass size distributions of the individual components (Fig. S2), so the internal mixing assumption is appropriate. Furthermore, for the aerosol considered here, organic species are highly oxidized, and the humidity levels are above 40%, so that phase separation or semi-solid conditions are not expected to frequently occur - hence acidity inferences using the single-phase metastable aerosol assumption tend to work well (see ref. [6], and references therein).

The results of the thermodynamic analysis are then combined with the conceptual framework of ref. [5] to identify the chemical domains of PM mass sensitivity to HNO_3 and NH_3 availability for this observational dataset. These sensitivity domains are characterized as: i) primarily NH_3-sensitive; ii) primarily HNO_3-sensitive; iii) combined NH_3 and HNO_3 sensitive; and, iv) HNO_3/NH_3 insensitive. This thermodynamically consistent approach enables us to directly determine how change in gas phase species will elicit a change in PM mass. As it pertains to the KORUS-AQ campaign, we adopt the ref. [5] threshold value for nitrate and ammonia partitioning that separates each regime at the 10% level. For example, for nitrate this means that when more than 10% of the total nitrate is in the particle phase, we would expect PM responses to NO_3^- precursors to be significant.

2.3 *Nitrate Partitioning Constrained pH (NPC-pH)*

When the thermodynamic model is run in forward mode, input of semi-volatile species (*i.e.* those that can exist in particle- or gas-phase) are assumed to be total gas and particle concentrations. As in this study, when NH_3 data is unavailable, the total NH_3 will be lower than the true value, as some fraction of the total NH_3 is actually in the gas phase. In these cases, neglecting gas-phase NH_3 results is an overestimation of particle acidity – often by about 1 pH unit.[36] It is therefore highly desirable to have an approach that can provide more realistic estimates of aerosol pH.

To address the above issue, past studies have proposed an iterative approach to calculate pH and gas phase ammonia data (*e.g.* ref. [41]) that involves running ISORROPIA-II (without gas-phase ammonia) to retrieve the predicted equilibrium gas phase ammonia concentration from the model output. This equilibrium NH_3 along with the measured NH_4^+ is then used as total ammonia input for the next ISORROPIA-II iteration (which eventually adds some mass to the system), holding all other input values constant. After each such iteration, convergence is checked by examining whether the values of gas-phase NH_3 agree to within a predefined criterion. This method, however, is unconditionally unstable, *i.e.* the method does not converge when an increasingly strict criterion is used (see Fig. 2 for a schematic).

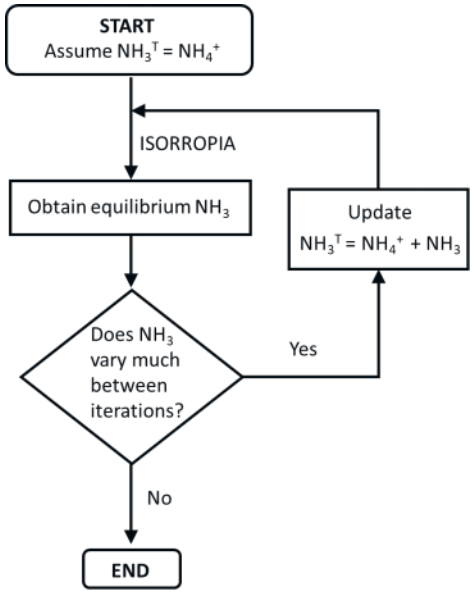

Fig. 2. Method from ref. [41] for constraining aerosol pH in the absence of NH_3 data.

To demonstrate this, Fig. 3 presents how pH and gas-phase NH_3 change with iteration; a stable algorithm would eventually converge to values that do not change with iteration; in reality NH_3 and pH increase monotonically (but initially with very small increments per iteration – which can be misinterpreted as convergence) without a bound. This instability is not unique to ISORROPIA-II, but inherent to the algorithm and should apply to any thermodynamic model, as the amount of total ammonia with every iteration increases – without any bound. Applying a less

strict upper bound would result in an arbitrary estimate of total ammonia, which requires some prior knowledge on NH_3 levels to provide realistic values of pH (which is what ref. [41] adopted).

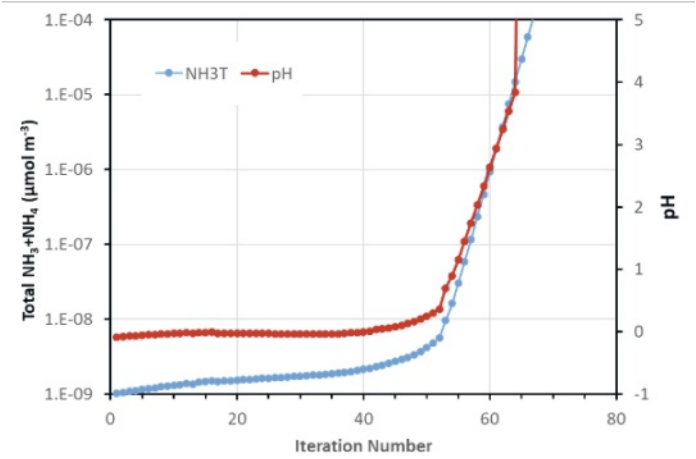

Fig. 3. Total ammonia (blue) and pH (red) as a function of iteration number using the algorithm from ref. [41].

As an alternative to the ref. [41] algorithm, we propose a method to infer pH calculations from thermodynamic analysis of observations when NH_3 data are lacking. This approach involves using an algorithm that is tied to the observed nitrate/nitric acid partitioning (hereafter referred to as 'nitrate partitioning constrained pH', NPC-pH) to infer gas-phase NH_3 concentrations required for plausible pH predictions. Fig. 4 summarizes the methodology behind this approach. The observed NH_4^+, total nitrate, and nitrate partitioning fraction, $\varepsilon(NO_3)$ – defined as the fraction of total nitrate (gas + aerosol) present in the aerosol phase – are used as input to an iterative algorithm that determines the value of gas-phase NH_3 that, together with the observed value of NH_4^+, temperature, and relative humidity reproduces the observed $\varepsilon(NO_3)$ to some predetermined level of accuracy. The thermodynamic calculations required for each step in the iterative procedure are done with ISORROPIA-II. Upon convergence (here, to within 10^{-6} between iterations), particle liquid water, H^+_{air} concentration, and particle pH are obtained and used for further analysis. In the following, we assess the predicted pH with NPC-pH, which together with aerosol liquid water content is needed to determine an effective PM control strategy.

Nitric acid can condense onto fine mode and coarse particles containing non-volatile cations (from seasalt or dust). Because of this, nitrate may over time volatilize and recondense onto coarse mode cations forming nonvolatile species (in the form of $Ca(NO_3)_2$, $NaNO_3$ and other salts). This disequilibrium will lead to a gas phase HNO_3 concentration which is lower than the equilibrium value expected from the PM_1 composition and higher than the corresponding value based on the coarse mode composition. Given that the equilibration timescale of submicron aerosol is much smaller than for coarse mode particles, the degree of disequilibrium between the PM_1 nitrate and gas-phase HNO_3 is much smaller than that for coarse mode nitrate. We therefore assume that the PM_1 semi-volatile inorganic species (NO_3^-, NH_4^+) are in equilibrium with their gas phase components (HNO_3, NH_3). Analysis carried out by ref. [14] supports this approach.

2.4 *Data Selection and Analysis*

Data points were filtered for conditions where ambient relative humidity (RH) fell within the range of 45-95%, and flight altitude below 1 km which is often within the boundary layer and most relevant from an air quality perspective (the RH in the sampling line was often significantly lower, but exposure to these low levels of humidity is too short to have a significant impact on semi-volatile nitrate and ammonium[42,43]). The RH range was chosen to ensure robust estimations from the thermodynamic model. Data for RH > 95% were excluded owing to the exponential growth in particle liquid water with RH, which leads to high W_i and subsequently large pH uncertainty owing to propagation of RH uncertainties.[36] Guo *et. al.*[41] suggests that below RH of 40%, pH estimations are subject to considerable uncertainty owing to the low aerosol liquid water and other uncertainties, which limits the ability to capture the observed partitioning of nitrate and other species. Data points above the boundary layer are possibly included in the analysis, but the low RH values typically exclude them. From this filtering process, a total of 11 of the total flights were analyzed and are summarized in Table S2.

3. Results

3.1 *Sensitivity Studies to Evaluate the New NPC-pH Algorithm*

The NPC-pH algorithm for predicting pH without NH_3 data was assessed based on a synthetic dataset for which aerosol is in perfect thermodynamic equilibrium. To this dataset, random variability is added to the concentration of semi-volatile species (within a predefined but relatively wide range). The NPC-pH algorithm was applied to the original and noisy synthetic data sets, to predict pH. The aerosol acidity obtained from NPC-pH was then compared to the pH of the initial data where the aerosol was in equilibrium with all species. The robustness of the acidity to noise level is important, especially given that aerosol semi-volatile species could be in disequilibrium.

The synthetic data was constructed of aerosol precursor values relevant for KORUS-AQ conditions: total NO_3 concentration ranged from 0.2 to 110 µg m^{-3} allowing for $\varepsilon(NO_3)$ to range

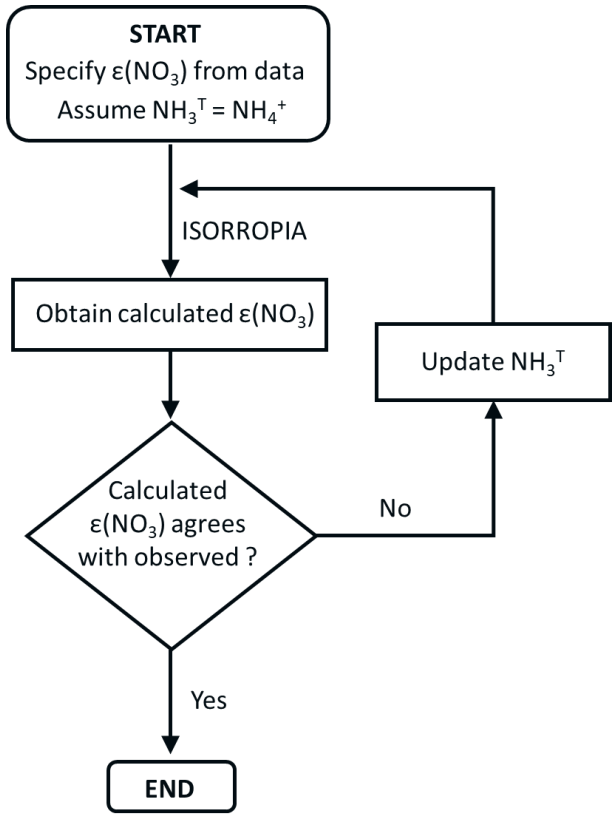

Fig. 4. The nitrate partitioning constrained pH (NPC-pH) method to obtain aerosol pH from nitrate partitioning observations.

from 0-0.95. Total SO_4 and total NH_4^+ concentrations ranged from 0.1-10 μg m^{-3} and 0.2-110 μg m^{-3}, respectively, and $\varepsilon(NH_4)$ ranged from 0-1. The total Cl concentration was kept constant at 0.50 μg m^{-3} and NVC concentrations were set to zero. Temperature was kept constant at 298K, and the RH ranged from 45-95%. Comparing the equilibrium partitioning retrieved from the synthetic data (without added noise) to that generated from the algorithm resulted in nearly perfect agreement between the two quantities, when $\varepsilon(NO_3)$ was greater than about 40% (Fig. 5). Higher sensitivity of low $\varepsilon(NO_3)$ values to pH and gas-phase NH_3 results in more scatter in $\varepsilon(NO_3)$ generated from the algorithm for $\varepsilon(NO_3)$ < 0.4. Average pH for the whole synthetic dataset for equilibrium and NPC-pH method are 2.14 ± 1.33 and 2.26 ± 1.25, respectively while the average LWC for equilibrium and NPC-pH method are 42.50 ± 137.85 μg m^{-3} and 42.25 ± 137.93 μg m^{-3}, respectively. The large standard deviation is a result of a wide range of conditions tested during the analysis.

To ascertain how uncertainties in nitrate partitioning (*i.e.* deviations from thermodynamic equilibrium) would impact pH inferences from NPC-pH, random noise at the 1-50% level is added to the original $\varepsilon(NO_3)$ values from the synthetic dataset. Reapplication of NPC-pH to the noisy datasets then quantify the effect of this noise to the inferred pH. The method used to add noise is shown in Equations 2 and 3

$$X = 2\Phi\left(-\frac{1}{2} + Rnd\right)\varepsilon(NO_3) \quad (2)$$

$$\varepsilon(NO_3)_{Rnd} = \varepsilon(NO_3) + X \quad (3)$$

Where $\varepsilon(NO_3)_{Rnd}$ is $\varepsilon(NO_3)$ with added random noise X that is symmetrical about zero and scaled to the magnitude of $\varepsilon(NO_3)$; Φ is the maximum fractional noise level (ranging from 0.01-0.5 to express a noise level of 1-50%) and *Rnd* is a random number between 0 and 1, generated by the 'rand()' pseudorandom number generator available in the Matlab® environment.

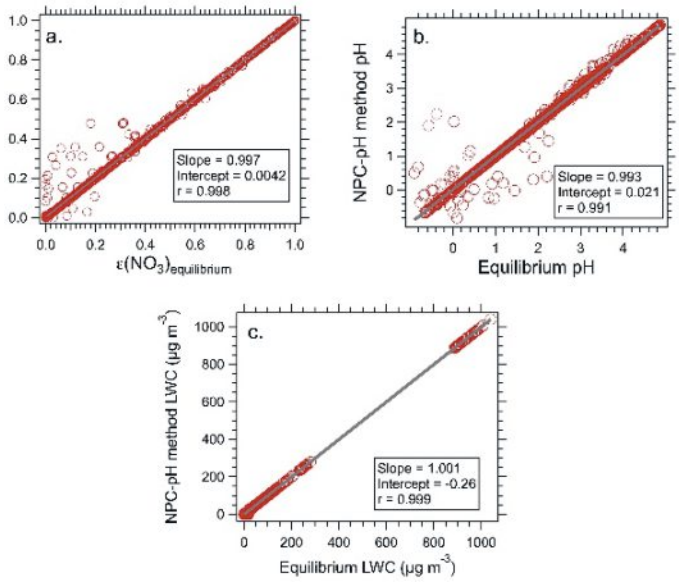

Fig. 5. Comparison of equilibrium nitrate partitioning retrieved from synthetic data *vs.* the value from the NPC-pH method. Meteorological conditions in the synthetic dataset cover an RH of 45-95%, Temperature 298K and SO_4, NO_3^T, NH_4^T of 0.1-10 μg m^{-3}, 0.2-110 μg m^{-3}, and 0.2-110 μg m^{-3}, respectively. Non-volatile cation concentrations were set to zero, and Cl- concentration was kept constant at 0.5 μg m^{-3}.

Results from this sensitivity analysis reveal that a 50% relative error in $\varepsilon(NO_3)$ resulted in an average absolute error in pH of 0.28±0.45 units, and explained as follows. Fig. 6 presents $\varepsilon(NO_3)$, $\varepsilon(NH_4)$ and pH for T= 288 K, and with average ISORROPIA-predicted liquid water content (13.78±10.52 μg m^{-3}) and activity coefficients (0.125 and 1.794 for $\gamma_{NO_3^-}$-γ_{H^+} and γ_{H^+}/$\gamma_{NH_4^+}$, respectively) derived from the KORUS-AQ flight data analysis (Table S1). In the blue region, where $\varepsilon(NO_3)$ approaches 1, we observe that a small uncertainty in $\varepsilon(NO_3)$ can result in significant changes to pH. In the pink region, however, we would expect that even large changes in $\varepsilon(NO_3)$ would only result in minor changes to pH. Evaluating 0.2< $\varepsilon(NO_3)$ <0.8 from the synthetic data resulted in an average absolute error in pH of 0.21±0.15 units. Therefore, pH predictions using this method are reasonably accurate, especially when considering the inherent uncertainty of pH inferences using thermodynamic models[6] and the low sensitivity of pH to NH_3 inferences error (about a factor of 10 error in NH_3 provides a pH error of 1 unit, regardless of acidity regime.[44,45]

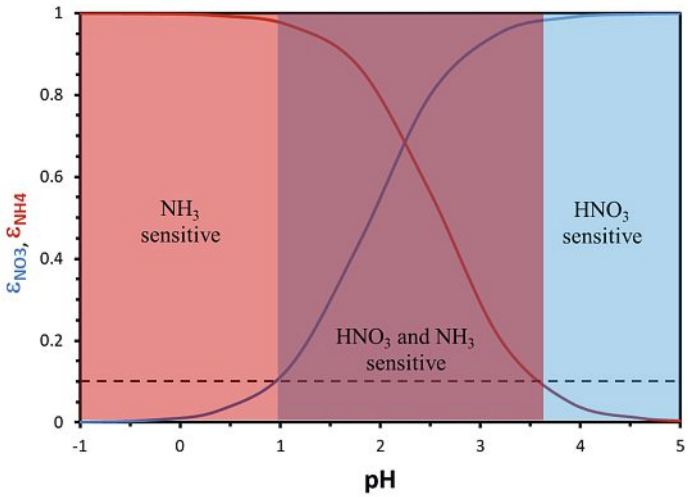

Fig. 6. Particle phase fraction of total nitrate, (NO_3^-) (blue curve) and total ammonium, (NH_4^+) (red curve) versus pH for a temperature of 288 K and an aerosol liquid water content of 13.78 μg m^{-3}. The pink zone is a region where PM is sensitive to both HNO_3 and NH_3. Following the approach of ref. [5], the dotted black line represents a pre-defined threshold, below which the aerosol is deemed insensitive to changes in NH_3 and/or HNO_3.

3.2 *Aerosol Acidity During KORUS-AQ*

KORUS-AQ integrated aircraft and ground-based measurements, and satellite observations. The campaign was conducted over South Korea (33 and 39 °N, 124 and 130 °E) and the Yellow Sea during the months of May and June in 2016. Flight tracks for the DC-8 during KORUS-AQ are shown in Fig. 7, colored by measured concentrations of NO_3^-. Most flights focused on the western region (35 and 38 °N, 126 and 127 °E) of South Korea extending into the Yellow Sea. Major emitters of NO_X are the Taean coal power plant (36.90 °N, 126.23 °E), Dangjin power plant (37.06 °N, 126.51 °E), and Yeongheung power station (37.24 °N, 126.44 °E) – which are all within the region of observed high nitrate concentrations.[46-48] Increased nitrate levels observed in Table S1 for Asia are most likely the result of emissions from vehicular traffic and power plants, and active photochemistry[2] and nighttime nitrate formation from N_2O_5 hydrolysis.[4] More details on KORUS-AQ flights can be found in Nault *et al.*[2]

Measurements of HNO_3 and NO_3^- indicate that $\varepsilon(NO_3)$ most of the time (approximately 92%; Fig. S4) falls between 0.1 and 0.9, indicating that aerosol nitrate levels will be sensitive to pH (*i.e.* reside in the 'sensitivity window'[37] Fig. 6). Of the remaining 8%,

approximately 6% of these partitioning values fall below 0.1, while 2% of all nitrate partitioning measurements were greater than 0.9, where nitrate partitioning is expected to be less sensitive to pH changes. Given this and the sensitivity analysis of Section 3.1, the NPC-pH algorithm can provide robust estimates of aerosol pH for the majority of the KORUS-AQ data. We find that the average pH for all flights was 2.43±0.68 (Table S1), while the average acidity between flights varied between 1.74 and 2.90 (Table S2). These pH levels are similar to what has been reported by others in the region for spring/summertime conditions; spring in Beijing, China (pH range= 1.8-4.3) (ref. [6] and references therein).

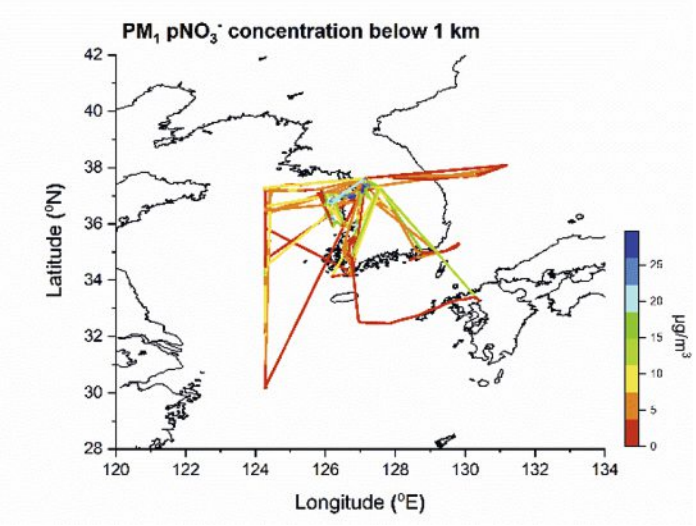

Fig. 7 (a) Flight trajectories for altitudes below 1km during KORUS-AQ, color mapped by NO_3^- levels. Highest concentrations of NO_3^- observed near Seoul, for which NO_x emissions are dominated by the transportation and energy industries. (b) NO_x emission sources in Korea labelled by industry.

The inorganic fraction of the KORUS-AQ aerosol is dominated by sulfate, ammonium, and nitrate (Fig. 1). Since, as already mentioned in the methods, the relative mass concentrations of NVCs to other major inorganic ion components are low, we assume the formation of nonvolatile salts (*e.g.* $Ca(NO_3)_2$ and $Na(NO_3)$) negligibly impact the pH derived from nitrate partitioning. This assumption is valid as the pH calculated using SAGA measurements of NVCs (which includes aerosol with size up to 4.1 μm) is within 1% of that predicted, consistent with the impact suggested in ref. [14]. We also do not consider the contribution of organic nitrates to the total amount of nitrates (which constitute less than 10% of the total nitrate, hence have a minimal impact on liquid water content and pH, based on the analysis in Section 3.1).

Particle pH is affected by several coupled variables such as particle nitrate and nitrate partitioning levels. Higher ambient particle pH is often associated with higher concentrations of particle nitrate.[14] This occurs when nitrate aerosol (usually in the form of ammonium nitrate) dominates the aerosol liquid water content; in such situations, the aerosol can contain considerable amounts of aerosol water but maintain small amounts of H^+ in solution – as it tends to combine with NO_3^- to form volatile HNO_3. In contrast, when aerosol liquid water is controlled by hygroscopic sulfates, significant amounts of H^+ can exist in solution (*e.g.* from the semi-volatile partitioning of NH_4^+ to form NH_3) as its tendency to associate with HSO_4^-, SO_4^{2-} is relatively weak and sulfates are involatile. This general effect of higher (lower) pH associated with higher (lower) NO_3 has been seen in a number of other field campaigns (see comparisons in Table S1). In Cabauw, Netherlands during the summer Guo et al.[38] reported an $\varepsilon(NO_3)$ of 88%, with a corresponding pH of 3.3±0.5. Both quantities are higher than the values found for the KORUS-AQ campaign. The pH of aerosol in Beijing, China in the summer was found to be 3.9±1.3 for nitrate levels that are higher than those measured for the South Korean data (Table S1).

3.3 *Acidity and PM Sensitivity Regimes to NH_3 and HNO_3 During KORUS-AQ*

Nenes *et al.*[5] developed a framework that allows PM sensitivity to NH_3 and HNO_3 availability to be determined from aerosol acidity and liquid water content. This framework directly determines effective PM reduction policies – which is important given recent work identifying NH_3 reductions over other policies (*e.g.* NO_X and SO_X reductions)[49,50] as the most effective for PM reductions, and the dominance of PM in the region by ammonium and nitrate (22.2 and 36.6%, respectively; Fig. 1). PM can refer to any size cut, but mostly refer to PM_1 or $PM_{2.5}$ – the former being the one used in this study.

In its simplest form, the Nenes *et al.* framework[5] is expressed in terms of a 'policy map' (Figs. 8 and 9) characterized by four distinct regimes: one, shaded pink, where $\varepsilon(NO_3)$ is small and $\varepsilon(NH_4)$ is large (*i.e.* the majority of nitrate resides in the gaseous phase and ammonium in the particle phase, defined by a relevant threshold); here PM mass responds proportionally to changes in the total ammonia but tends to be insensitive to total nitrate changes. For this reason, Nenes *et al.*[5] characterize PM in this regime as being 'NH_3 sensitive'. The opposite is seen in the blue-shaded regime, as the majority of nitrate resides in the aerosol phase and ammonia in the gas phase. For this reason, Nenes *et al.*[5] characterize PM in this region as being 'HNO_3 sensitive'. In both acidity regimes, partitioning may not be strongly affected by pH changes, therefore uncertainties in its exact value carry minor implications for PM sensitivity to available ammonia and nitrate. In the purple acidity domain, however, which Vasilakos *et al.*[37] term 'sensitivity window', PM tends to respond to both HNO_3 and NH_3 emissions, as an important fraction of both species is in the aerosol phase.[5] Here, rather precise knowledge of aerosol pH is important – as variations to within one unit usually imply a large change in the partitioning fraction for each semi-volatile species, hence PM sensitivity. The fourth domain, colored white, is characterized by low nitrate and ammonium partitioning fraction, and PM is then relatively insensitive to changes in NH_3 and HNO_3 availability.

From the histogram of observed nitrate partitioning (Fig. S4), we expect a large fraction of the data to lie in the HNO_3-NH_3

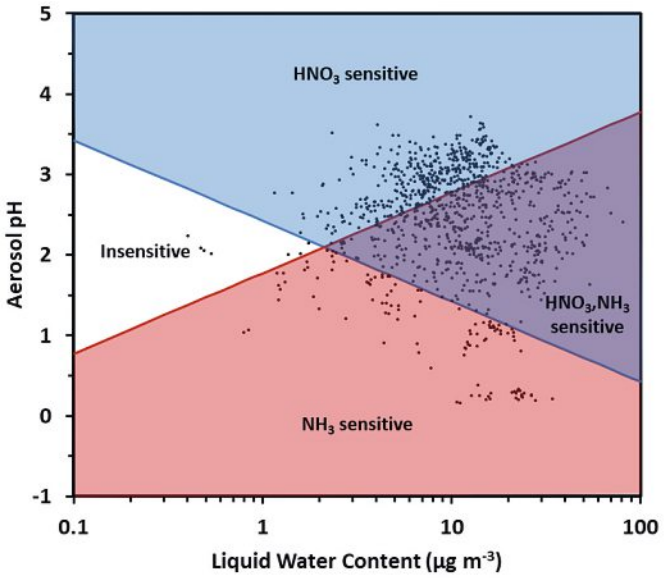

Fig. 8. Chemical domains for entire KORUS-AQ study data. Larger fraction of data falls in HNO_3 sensitive region as a result of moderate-high values of nitrate partitioning.

sensitive domain. As distribution of nitrate partitioning is toward the high end of $\varepsilon(NO_3)$ for the study (average nitrate partitioning value of 58±24%), PM_1 reductions would be sensitive to reductions in HNO_3 – hence NO_X reductions. Indeed, if the pH and aerosol liquid water content for the KORUS-AQ data are plotted on the policy map (Fig. 8), the data reside in the domain where HNO_3 or a mix of HNO_3-NH_3 controls are generally the most effective routes for reduction of inorganic PM_1 mass for the time period of the study.

The above analysis can be further expanded to consider only PM levels above a regulatory mass threshold, as PM control policies are most effective when relevant for the high PM levels seen in pollution events. To assess this, we plot all the available data on the policy map, but with points color-coded with PM level (Fig. 10). For PM levels exceeding *e.g.* 30 µg m^{-3}, HNO_3 is always an effective control strategy, while NH_3 is effective for about half the points. The relatively fewer cases that fall into the NH_3-sensitive domain are characterized by low PM levels, hence less important to control. Given that dry deposition dominates the loss of boundary layer PM during haze episodes, and the expected low deposition rate of nitrate when $\varepsilon(NO_3)$ is relatively large Nenes *et al.*[51] further emphasize the need to control NO_X, as such conditions favor the rapid accumulation of available HNO_3 – and buildup of the high levels of NO_3-seen in the observations (Fig. 1).

It should be pointed out that although the analysis determines effective emissions controls for data collected within the 1 km from ground level, we do not imply that policies should be applied only at the local level. It is well known that long-range transport of pollutants can bear a considerable contribution to PM levels, and also help precondition the aerosol and its sensitivity regime by affecting its LWC and pH. Therefore, an effective policy should ideally combine reductions in emissions that address both remote and local sources. Towards this a full back-trajectory analysis of each observation would provide valuable insights on the origin and relative importance of long-range transport – but is left for a future study.

4. Summary and Broader Implications

Accurate estimates of atmospheric aerosol acidity are important for understanding a number of atmospheric processes sensitive to pH. Here, we present a method – called NPC-pH - for

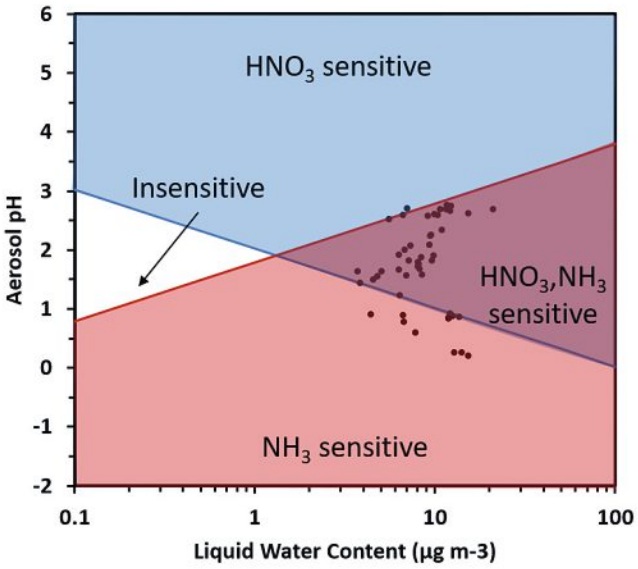

(a)

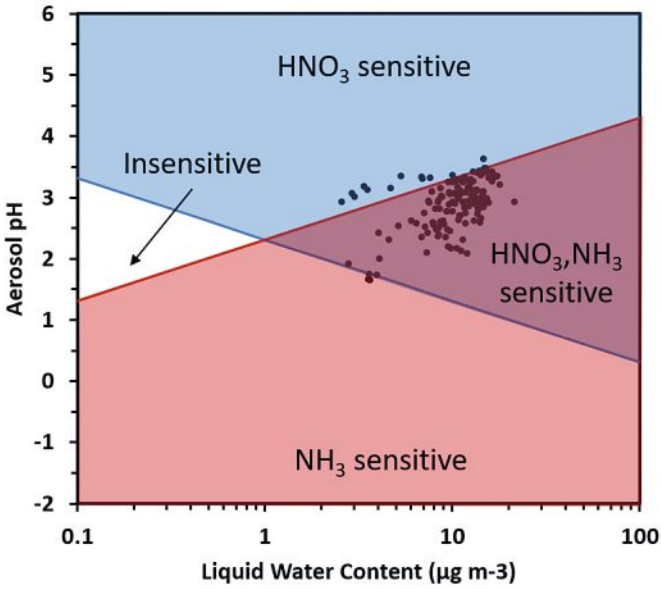

(b)

Fig. 9. Chemical domains for (a) flight 15 and (b) flight 19. For Flight 15, a significant number of its data points are characterized by low nitrate partitioning values (approx. 30%). Flight 19 is characterized by high levels of particle nitrate, and moderate to high levels of nitrate partitioning. For these reasons, PM would be sensitive to NH_3 (HNO_3) for flights 15 and 19, respectively.

estimating aerosol pH, through thermodynamic analysis of observations that lack gas-phase ammonia measurements. NPC-pH is based on the observed gas-to-particle partitioning of nitrate in the absence of ammonia measurements and is shown to perform much better than a previously proposed algorithm that iterated for total ammonia (using aerosol ammonium as an initial guess), as the latter is shown to be unconditionally unstable. NPC-pH is also shown to provide robust pH levels that are relatively insensitive to nitrate partitioning errors.

Applying NPC-pH to airborne observations collected from the NASA/NIER KORUS-AQ field campaign in South Korea resulted in pH predictions (pH=2.43 ± 0.68) that are consistent with published estimates in this region and season. The pH and LWC

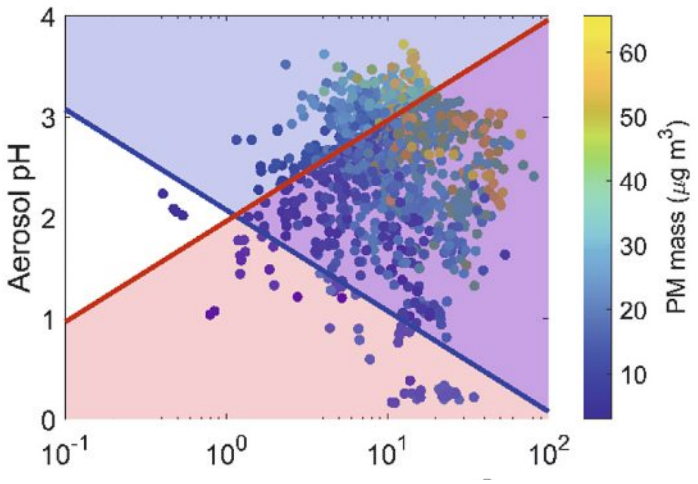

Fig. 10. Chemical domains for entire KORUS-AQ study data, with symbols colored by the value of PM.

calculated from our thermodynamic analysis and the approaches of refs. [50,51] determine the 'chemical regime' of PM sensitivity to ammonia and nitrate availability, and, 'dry deposition velocity regime' of inorganic nitrogen (which controls the lifetime, hence accumulation, of nitrate in the boundary layer during haze episodes). For KORUS-AQ, we found that the aerosol formation is often in the NH_3 and HNO_3-sensitive or HNO_3-sensitive zone, while a small fraction (4%) of the points fall in NH_3-limited region near the Yellow Sea, Jeju Island, Busan and Eastern Sea. Nevertheless, when PM levels are high, the data always lies in the HNO-sensitive or HNO_3-NH_3 sensitive region. Under these conditions, we conclude that HNO_3 reductions prove to be the most effective for all conditions examined, and that NH_3 emissions would only partially be effective in reducing PM levels – especially given that during pollution episodes, the pH and LWC levels promote rapid accumulation of nitrate aerosol in the boundary layer owing to its slow dry deposition.[51] A complete in-depth analysis of the complex chemistry and contributions of different sources however is required to fully assess the most effective NO_X emission controls to reduce HNO_3 production, as well as understanding the origin of NO_X (local *vs.* long-range transport) for a most effective policy. Towards this, back-trajectory analysis and regional modeling can provide the insights required for this important analysis. Source attribution information can also be represented on the policy maps shown here to understand their role in shaping the acidity, liquid water, and PM sensitivity/deposition regimes to further refine types of policies that could be effective during pollution episodes. Although much of the measurements analyzed here are close to ground, considering the difference in conditions between ground-level and aloft (particularly the effects of temperature and RH) on the conclusions derived will always be an important aspect that should be considered. And, as our algorithm is applied to other ambient data sets in the future, we suggest that a future study focusing on lab experiments dedicated to assessing the NPC-pH method stringently would be highly desirable.

Despite the benefits of controlling PM formation to reduce ammonium-nitrate aerosol and PM mass, we must consider that the acidity domain can significantly affect other processes and sources of aerosol toxicity.[52,53] It was shown that acid-driven dissolution of transition metals (*e.g.* Fe, Cu) can potentiate health effects such as cardiovascular morbidity and mortality through oxidative stress.[54,55] If emissions controls, in an attempt to reduce PM levels also lead to reduction in pH, this may unintentionally increase aerosol toxicity with adverse health effects in humans. Lastly, increased aerosol acidity can impact the deposition pattern of reactive nitrogen[51] and bioavailability of micronutrients (*e.g.* Fe, P) with both synergistic and/or antagonistic effects on remote ecosystems.[56]

Acknowledgements

This work was supported by NASA grant NNX16AE19G (KORUS-AQ), from PyroTRACH (ERC-2016-COG) funded from H2020-EU.1.1. - Excellent Science - European Research Council (ERC), project ID 726165 and the Swiss National Science Foundation project 192292, Atmospheric Acidity Interactions with Dust and its Impacts (AAIDI). JLJ, PCJ, and BAN (AMS) were supported by NASA grants NNX15AT96G, 80NSSC19K0124, and 80NSSC18K0630. JDC, MKJ, AT, and POW (Caltech) were supported by NASA grants NNX15AT97G. The ISORROPIA-II thermodynamic equilibrium code is available at http://isorropia.epfl.ch. KORUS-AQ data is available at https://www-air.larc.nasa.gov/cgi-bin/ArcView/korusaq

Author Contributions

II was responsible for the thermodynamic analysis of the ambient data, contributed to the ammonia estimation algorithm and wrote the initial draft of the manuscript with significant contributions by AN and RW. AN handled all the responses and revisions. AN developed the conceptual framework used here for understanding the sensitivity of $PM_{2.5}$ to total nitrate and ammonia, the tools to include the ambient data on the acidity maps and also demonstrated the unconditional instability of the original NH_3 iteration algorithm of Guo *et al*. (2016). AN and RW were involved in planning and supervision of the work. All authors provided data and feedback on the analysis approach, commented and contributed to the manuscript text.

Received: September 16, 2024

[1] H. Kim, Q. Zhang, J. Heo, *Atmos. Chem. Phys*. **2018**, *18*, 7149, https://doi.org/10.5194/acp-18-7149-2018.
[2] B. A. Nault, P. Campuzano-Jost, D. A. Day, J. C. Schroder, B. Anderson, A. J. Beyersdorf, D. R. Blake, W. H. Brune, Y. Choi, C. A. Corr, J. A. de Gouw, J. Dibb, J. P. DiGangi, G. S. Diskin, A. Fried, L. G. Huey, M. J. Kim, C. J. Knote, K. D. Lamb, T. Lee, T. Park, S. E. Pusede, E. Scheuer, K. L. Thornhill, J. H. Woo, J. L. Jimenez, *Atmos. Chem. Phys*. **2018**, *18*, 17769, https://doi.org/10.5194/acp-18-17769-2018.
[3] RSSR: Introduction to the KORUS?AQ Rapid Science Synthesis Report, https://espo.nasa.gov/sites/default/files/documents/KORUS-AQ-ENG.pdf, **2016**.
[4] C. E. Jordan, J. H. Crawford, A.J . Beyersdorf, T. F. Eck, H. S. Halliday, B. A. Nault, L. S. Chang, R. Park, G. Lee, H. Kim, S. Cho, H. J. Shin, J. H. Lee, J. Jung, D. S. Kim, M. Lee, T. Lee, A. Whitehill, J. Szykman, M. K. Schueneman, P. C. Jost, J. L. Jimenez, J. P. DiGangi, G. S. Diskin, B. E. Anderson, R. H. Moore, L. D. Ziemba, M. A. Fenn, J. W. Hair, R. E. Kuehn, R. E. Holz, G. Chen, K. Travis, M. Shook, D. A. Peterson, K. D. Lamb, J. P. Schwarz, *Elementa* **2020**, *8*, 28, https://doi.org/10.1525/elementa.424.
[5] A. Nenes, S.N. Pandis, R.J. Weber, A. Russell, *Atmos. Chem. Phys*. **2020**, *20*, 3249, https://doi.org/10.5194/acp-20-3249-2020.
[6] H. O. T. Pye, A. Nenes, B. Alexander, A. P. Ault, M. C. Barth, S. L. Clegg, J. L. Collett Jr, K. M. Fahey, C.J . Hennigan, H. Herrmann, M. Kanakidou, J. T. Kelly, I. T. Ku, V. F. McNeill, N. Riemer, T. Schaefer, G. Shi, A. Tilgner, J. T. Walker, T. Wang, R. J. Weber, J. Xing, R. A. Zaveri, A. Zuend, *Atmos. Chem. Phys*. **2020**, *20*, 4809, https://doi.org/10.5194/acp-20-4809-2020.
[7] C. J. Hennigan, J. Izumi, A. P. Sullivan, R. J. Weber, A. Nenes, *Atmos. Chem. Phys*. **2015**, *15*, 2775, https://doi.org/10.5194/acp-15-2775-2015.
[8] S. M. Song, W. Gao, J. Xu, G. Shao, S. Shi, Y. Wang, Y. Wang, Y. Sun, M. B. McElroy, *Atmos. Chem. Phys*. **2018**, *18*, 7423, https://doi.org/10.5194/acp-18-7423-2018.
[9] S. Wang, J. Nan, C. Shi, Q. Fu, S. Gao, D. Wang, H. Cui, A. Saiz-Lopez, B. Zhou, *Scientific Reports* **2015**, *5*, 15842, https://doi.org/10.1038/srep15842.
[10] L. Zhu, D. K. Henze, J. O. Bash, G.-R. Jeong, K. Cady-Pereira, M. Shephard, M. Luo, F. Paulot, S. Capps, *Current Pollution Reports* **2015**, *1*, 95, https://doi.org/10.1007/s40726-015-0010-4.
[11] M. L. Dawson, V. Perraud, A. Gomez, K. D. Arquero, M. J. Ezell, B. J. Finlayson-Pitts, *Atmos. Meas. Tech*. **2014**, *7*, 2733, https://doi.org/10.5194/amt-7-2733-2014.
[12] K. Osada, S. Ueda, T. Egashira, A. Takami, N. Kaneyasu, *Aerosol and Air Quality Research*, **2011**, *11*, 170, https://doi.org/10.4209/aaqr.2010.11.0101.
[13] R. J. Yokelson, T. J. Christian, I. T. Bertschi, W. M. Hao, *J. Geophys. Res.: Atmos*. **2003**, *108,* 4649, https://doi.org/10.1029/2003JD003549.

[14] H. Guo, A. Nenes, R. J. Weber, *Atmos. Chem. Phys*. **2018**, *18*, 17307, https://doi.org/10.5194/acp-18-17307-2018.
[15] P. F. DeCarlo, E. J. Dunlea, J. R. Kimmel, A. C. Aiken, D. Sueper, J. Crounse, P. O. Wennberg, L. Emmons, Y. Shinozuka, A. Clarke, J. Zhou, J. Tomlinson, D. R. Collins, D. Knapp, A. J. Weinheimer, D. D. Montzka, T. Campos, J. L. Jimenez, *Atmos. Chem. Phys*. **2008**, *8*, 4027, https://doi.org/10.5194/acp-8-4027-2008.
[16] E. J. Dunlea, P. F. DeCarlo, A. C. Aiken, J. R. Kimmel, R. E. Peltier, R. J. Weber, J. Tomlinson, D. R. Collins, Y. Shinozuka, C. S. McNaughton, S. G. Howell, A. D. Clarke, L. K. Emmons, E. C. Apel, G. G. Pfister, A. van Donkelaar, R. V. Martin, D. B. Millet, C. L. Heald, J. L. Jimenez, *Atmos. Chem. Phys*. **2009**, *9*, 7257, https://doi.org/10.5194/acp-9-7257-2009.
[17] J. R. Kimmel, D. K. Farmer, M. J. Cubison, D. Sueper, C. Tanner, E. Nemitz, D. R. Worsnop, M. Gonin, J. L. Jimenez, *Int. J. Mass Spect.* **2011**, *303*, 15, https://doi.org/10.1016/j.ijms.2010.12.004.
[18] J. L. Fry, D. C. Draper, K. J. Zarzana, P. Campuzano-Jost, D. A. Day, J. L. Jimenez, S. S. Brown, R. C. Cohen, L. Kaser, A. Hansel, L. Cappellin, T. Karl, A. Hodzic Roux, A. Turnipseed, C. Cantrell, B. L. Lefer. N. Grossberg, *Atmos. Chem. Phys*. **2013**, *13*, 8585, https://doi.org/10.5194/acp-13-8585-2013.
[19] D. K. Farmer, A. Matsunaga, K. S. Docherty, J. D. Surratt, J. H. Seinfeld, P. J. Ziemann, J. L. Jimenez, *Proc. Nat. Acad. Sci.* **2010**, *107*, 6670, https://doi.org/10.1073/pnas.0912340107.
[20] Y. Chen, L. Xu, T. Humphry, A. P. Hettiyadura, K. Ovadnevaite, S. Huang, L. Poulain, J. C. Schroder, P. Campuzano-Jost, J. L. Jimenez, H. Herrmann, C. O'Dowd, E.A . Stone, N. L. Ng, *Environ. Sci. Technol.* **2019**, *53*, 5176, https://doi.org/10.1021/acs.est.9b00884.
[21] R. Bahreini, , B. Ervens, A. M. Middlebrook, C. Warneke, J. A. de Gouw, P. F. DeCarlo, J. L. Jimenez, C. A. Brock, J. A. Neuman, T. B. Ryerson, H. Stark, E. Atlas, J. Brioude, A. Fried, J. S. Holloway, J. Peischl, D. Richter, J. Walega, P. Weibring, A. G. Wollny, F. C. Fehsenfeld, *J. Geophys. Res.: Atmos*. **2009**, *114*, https://doi.org/10.1029/2008JD011493.
[22] L. G. Huey, D. J. Tanner, D. L. Slusher, J. E. Dibb, R. Arimoto, G. Chen, D. Davis, M. P. Buhr, J. B. Nowak, R. L. Mauldin, F. L. Eisele, E. Kosciuch, *Atmos. Environ*. **2004**, *38*, 5411, https://doi.org/10.1016/j.atmosenv.2004.04.037.
[23] S. Kim, L. G. Huey, R. E. Stickel, D. J. Tanner, J. H. Crawford, J. R. Olson, G. Chen, W. H. Brune, X. Ren, R. Lesher, P. J. Wooldridge, T. H. Bertram, A. Perring, R. C. Cohen, B. L. Lefer, R. E. Shetter, M. Avery, G. Diskin, I. Sokolik, *J. Geophys. Res.: Atmos.* **2007**, *112*, https://doi.org/10.1029/2006JD007676.
[24] L. G. Huey, P. W. Villalta, E. J. Dunlea, D. R. Hanson, C. J. Howard, *J. Phys. Chem*. **1996**, *100*, 190, https://doi.org/10.1021/jp951928u.
[25] C. Amelynck, N. Schoon, E. Arijs, *Int. J. Mass Spec*. **2000**, *203*, 165, https://doi.org/10.1016/S1387-3806(00)00321-3.
[26] J. D. Crounse, K. A. McKinney, A. J. Kwan, P. O. Wennberg, *Anal. Chem*. **2006**, *78*, 6726, https://doi.org/10.1021/ac0604235.
[27] J. E. Dibb, R. W. Talbot, E. M. Scheuer, G. Seid, M. A. Avery, H. B. Singh, *J. Geophys. Res.* **2003**, *108*, 8815, https://doi.org/10.1029/2002JD003111.
[28] G. S. Diskin, J. R. Podolske, G. W. Sachse, T. A. Slate, *Int. Soc. Optics Photonics* **2002**, https://doi.org/10.3334/ORNLDAAC/1937.
[29] C. Fountoukis, A. Nenes, *Atmos. Chem. Phys*. **2007**, *7*, 4639, https://doi.org/10.5194/acp-7-4639-2007.
[30] K. G. Dassios, S. N. Pandis, *Atmos. Environ*. **1999**, *33*, 2993, https://doi.org/10.1016/S1352-2310(99)00079-5.
[31] C. Fountoukis, A. Nenes, A. Sullivan, R. Weber, T. Van Reken, M. Fischer, E. Matías, M. Moya, D. Farmer, R. C. Cohen, *Atmos. Chem. Phys*. **2009**, *9*, 2141, https://doi.org/10.5194/acp-9-2141-2009.
[32] D. Day, W. Malm, *Atmos. Environ*. **2001**, *35*, 5169, https://doi.org/10.1016/S1352-2310(01)00320-X.
[33] J. H. Seinfeld, S. N. Pandis, John Wiley & Sons, Hoboken, 'Atmospheric Chemistry and Physics: From Air Pollution to Climate Change', 3rd Ed, **2016**
[34] P. E. Saide, M. Gao, Z. Lu, D. Goldberg, D. G. Streets, J. H. Woo, A. Beyersdorf, C. A. Corr, K. L. Thornhill, B. Anderson, J. W. Hair, A. R. Nehrir, G. S. Diskin, J. L. Jimenez, B. Nault, P. Campuzano-Jost, J. Dibb, E. Heim, K. D. Lamb, J. P. Schwarz, A. E. Perring, J. Kim, M. Choi, B. Holben, G. Pfister, A. Hodzic, G. R. Carmichael, L. Emmons, J. H. Crawford, *Atmos. Chem. Phys*. **2020**, *20*, 6455, https://doi.org/10.5194/acp-20-6455-2020.
[35] E. Heim, J. E. Dibb, E. Scheuer, P. Campuzano-Jost, B. A. Nault, J. L. Jimenez, D. Peterson, C. Knote, M. Fenn, J. Hair, A. J. Beyersdorf, C. Corr, B. E. Anderson, *Atmos. Environ*. **2020**, *224*, 117305, https://doi.org/10.1016/j.atmosenv.2020.117305.
[36] H. Guo, L. Xu, A. Bougiatioti, K. M. Cerully, S. L. Capps, J. R. Hite Jr, A. G. Carlton, S. H. Lee, M. H. Bergin, N. L. Ng, A. Nenes, R. J. Weber, *Atmos. Chem. Phys*. **2015**, *15*, 5211, https://doi.org/10.5194/acp-15-5211-2015.
[37] P. Vasilakos, A. Russell, R. J. Weber, A. Nenes, *Atmos. Chem. Phys*. **2018**, *18*, 12765, https://doi.org/10.5194/acp-18-12765-2018.
[38] H. Guo, R. Otjes, P. Schlag, A. Kiendler-Scharr, A. Nenes, R. J. Weber, *Atmos. Chem. Phys*. **2018**, *18*, 12241, https://doi.org/10.5194/acp-18-12241-2018.
[39] S. Zhu, K. N. Sartelet, Y. Zhang, A. Nenes, *J. Geoph. Res*. **2016**, *121*, https://doi.org/10.1002/2015JD024241.
[40] N. Riemer, A. P. Ault, M. West, R. L. Craig, J. H. Curtis, *Reviews of Geophysics* **2019**, *57*, 187, https://doi.org/10.1029/2018RG000615.
[41] H. Guo, A. P. Sullivan, P. Campuzano-Jost, J. C. Schroder, F. D. Lopez-Hilfiker, J. E. Dibb, J. L. Jimenez, J. A. Thornton, S. S. Brown, A. Nenes, R. J. Weber, *J. Geophys. Res. Atmos*. **2016**, *121*, 355, https://doi.org/10.1002/2016JD025311.
[42] T. Shingler, E. Crosbie, A. Ortega, M. Shiraiwa, A. Zuend, A. Beyersdorf, L. Ziemba, B. Anderson, L. Thornhill, A. E. Perring, J. P. Schwarz, P. Campazano-Jost, D. A. Day, J. L. Jimenez, J. W. Hair, T. Mikoviny, A. Wisthaler, A. Sorooshian, *J. Geophys. Res. Atmos*. **2016**, *121*, 4188, https://doi.org/10.1002/2015JD024498.
[43] H. Guo, J. Liu, K. D. Froyd, J. M. Roberts, P. R. Veres, P. L. Hayes, J. L. Jimenez, A. Nenes, R. J. Weber, *Atmos. Chem. Phys.* **2017**, *17*, 5703, https://doi.org/10.5194/acp-17-5703-2017.
[44] H. Guo, R. J. Weber, A. Nenes, *Scientific Reports*, **2017**, *7*, 12109, https://doi.org/10.1038/s41598-017-11704-0.
[45] S. Song, M. Gao, W. Xu, Y. Sun, D. R. Worsnop, J. T. Jayne, Y. Zhang, L. Zhu, M. Li, Z. Zhou, C. Cheng, Y. Lv, Y. Wang, W. Peng, X. Xu, N. Lin, Y. Wang, S. Wang, J. W. Munger, D. J. Jacob, M. B. McElroy, *Atmos. Chem. Phys*. **2019**, *19*, 1357, https://doi.org/10.5194/acp-19-1357-2019.
[46] J. H. Hong, J. Kim, W. Son, H. Shin, N. Kim, W. K. Lee, J. Kim, *Energy Policy* **2019**, *127*, 425, https://doi.org/10.1016/j.enpol.2018.11.055.
[47] S. Kafle, R. Parajuli, S. Bhattarai, S. H. Euh, D. H. Kim, *Renew. Sustain. Energy Rev*. **2017**, *73*, 1123, https://doi.org/10.1016/j.rser.2017.01.180.
[48] N. K. Kim, Y. P. Kim, Y. Morino, J. Kurokawa, T. Ohara, *Atmos. Environ*. **2013**, *77*, 496, https://doi.org/10.1016/j.atmosenv.2013.05.042.
[49] A. Pozzer, A. P. Tsimpidi, V. A. Karydis, A. de Meij, J. Lelieveld, *Atmos. Chem. Phys*. **2017**, *17*, 12813, https://doi.org/10.5194/acp-17-12813-2017.
[50] Z. Xu, M. Liu, Y. Song, S. Wang, L. Zhang, T. Xu, T. Wang, C. Yan, T. Zhou, Y. Sun, Y. Pan, M. Hu, M. Zheng, T. Zhu, *Atmos. Chem. Phys*. **2019**, *19*, 5605, https://doi.org/10.5194/acp-19-5605-2019.
[51] A. Nenes, S. N. Pandis, M. Kanakidou, A. G. Russell, S. Song, P. Vasilakos, R. J. Weber, *Atmos. Chem. Phys*. **2021**, *21*, 6023, https://doi.org/10.5194/acp-21-6023-2021.
[52] T. Fang, H. Guo, L. Zeng, V. Verma, A. Nenes, R. J. Weber, *Env. Sci. Tech*. **2017**, *51*, 2611, https://doi.org/10.1021/acs.est.6b06151.
[53] J. Wong, Y. Yang, J. Mulholland, A. G. Russell, S. Sarnat, A. Nenes, R. J. Weber, *Env. Sci. Tech*. **2020**, *54*, 7088, https://doi.org/10.1021/acs.est.0c00483
[54] J. T. Bates, R. J. Weber, J. Abrams, V. Verma, T. Fang, M. Klein, M. J. Strickland, S. E. Sarnat, H. H. Chang, J. A. Mulholland, P. E. Tolbert, A. G. Russell, *Env. Sci. Tech*. **2015**, *49*, 13605, https://doi.org/10.1021/acs.est.5b02967.
[55] A. J. Ghio, M. S. Carraway, M. C. Madden, *J. Tox. Environ. Health, Part B*, **2012**, *15*, 1, https://doi.org/10.1080/10937404.2012.632359.
[56] N. Meskhidze, W. L. Chameides, A. Nenes, G. Chen, *Geophys. Res. Lett*. **2003**, *30*, https://doi.org/10.1029/2003GL018035.